JOURNAL OF GEOPHYSICAL RESEARCH, VOL. 112, D07204, doi:10.1029/2006JD007702, 2007

Droplet growth by gravitational coagulation enhanced by turbulence: Comparison of theory and measurements

N. Riemer,[1] A. S. Wexler,[2] and K. Diehl[3]

Received 26 June 2006; revised 3 December 2006; accepted 29 December 2006; published 7 April 2007.

[1] While it is well known that cloud droplets grow in an inherently turbulent environment, the role of turbulence is only now being elucidated. To shed light on this issue, we compare published measurements of droplet growth by collision in turbulent flow with numerical simulations. Because the measurements demonstrate an accelerated growth under turbulent conditions compared to laminar ones, the data clearly cannot be reproduced using the well-established kernel for sedimentation under laminar conditions. By employing a collision kernel that has been recently derived from direct numerical simulations, we perform sensitivity studies and quantify the parameter ranges that are compatible with the experimental data. This experiment does not enable us to uniquely determine the model parameters but we were able to place constraints on the form of acceptable models that reproduce the experimental data successfully. Moreover, we gain insight into how laboratory experiments could be improved to aid model validation.

Citation: Riemer, N., A. S. Wexler, and K. Diehl (2007), Droplet growth by gravitational coagulation enhanced by turbulence: Comparison of theory and measurements, *J. Geophys. Res.*, *112*, D07204, doi:10.1029/2006JD007702.

1. Introduction

[2] Over the course of several decades, both experimental and theoretical studies have come to the conclusion that in-cloud turbulence enhances droplet growth [e.g., *Arenberg*, 1939; *Jonas and Goldsmith*, 1972; *Vohl et al.*, 1999; *Shaw*, 2003]. However, the adequate treatment of turbulence effects on droplet growth still represents a major gap in our understanding of cloud microphysics. While turbulence can modify both the collision of cloud droplets and the condensation of water vapor [e.g., *McGraw and Liu*, 2004], we will focus on the role that turbulence plays in the collision process.

[3] Air turbulence can impact droplet collision by at least four mechanisms. First, particle inertia leads to increased relative velocities and less correlated velocity directions (acceleration effect). Second, the wind field shear produces collisions between particles even with the same inertia (shear effect) [*Saffman and Turner*, 1956]. The acceleration and the shear effect are often referred to as the transport effect. Third, coagulation rates are enhanced due to local concentration increases if the particle response times are on the order of the Kolmogorov scale [*Maxey*, 1987]. For this phenomenon, the terms ''preferential concentration'' and ''accumulation effect'' are used. Fourth, turbulence can also impact the local droplet-droplet hydrodynamic interactions [*Pinsky et al.*, 1999; *Wang et al.*, 2005].

[4] Working toward a quantitative understanding, *Zhou et al.* [2001] developed a parameterization for the collision kernel based on the results of direct numerical simulations, advancing the concepts of *Sundaram and Collins* [1997] and *Kruis and Kusters* [1996]. This kernel accounts for both the transport effect and the accumulation effect. Because the current formulation of the kernel was derived for isotropic turbulence and does not include the effect of gravity, additional assumptions are required for its application to atmospheric conditions. Keeping this limitation in mind, we applied this kernel to realistic cloud situations showing that turbulence was essential to produce warm rain [*Riemer and Wexler*, 2005]. A comparison between the parameterization of Zhou et al. and the experimental data has not been performed so far, but is crucial to establishing its validity.

[5] One of the few experimental studies on the effect of turbulence on the collisional growth of drops has been performed by *Vohl et al.* [1999] and *Vohl* [2000]. Their study compares the collisional growth of the drops under laminar and turbulent conditions in a vertical wind tunnel. During the experiments, one collector drop with a radius larger than 50 μm was exposed to a cloud of small droplets, and therefore grew by collision, for 25 min in laminar and turbulent conditions.

[6] With the laboratory experiments, it is not possible to create the whole range of the turbulent kinetic energy spectrum present in atmospheric clouds. Consequently, only certain aspects of turbulence effects can be addressed. In this respect, the experiment of Vohl et al. is no exception. In particular, using $u' \sim 0.1$ m s^{-1} and $\epsilon \sim 500$ cm^2 s^{-3} as

[1]Marine Sciences Research Center, Stony Brook University, Stony Brook, New York, USA.
[2]Department of Mechanical and Aeronautical Engineering, Department of Civil and Enviromental Engineering, and Department of Land, Air, and Water Resources, University of California, Davis, California, USA.
[3]Institute of Atmospheric Physics, Johannes Gutenberg University, Mainz, Germany.

0148-0227/07/2006JD007702$09.00

typical values for the root mean square (r.m.s.) velocity fluctuation u' and the turbulent dissipation rate ϵ for the experimental conditions, the microscale Reynolds numbers R_λ in the wind tunnel are on the order of 10^2. This is 2 orders of magnitude smaller than in the atmosphere where $R_\lambda \sim 10^4$ applies [*Frehlich et al.*, 2004].

[7] The experiment is also limited to the investigation of a particular combination of collector and collected droplet sizes, namely a relatively large collector droplet in a cloud of small collected droplets. However, the advantages of this data set are that the effect of turbulence on collisional growth is isolated and other effects such as condensation, entrainment, and transport are excluded. To the authors' knowledge, this data set is the only one to date that allows a quantitative comparison with at least some aspects of parameterization of *Zhou et al.* [2001]. Therefore a comparison of the parameterization and the experiment represents an important step toward increasing the understanding of turbulent coagulation.

[8] An overview of the experimental setup and the method of our calculations is in section 2. In section 3, we will present our results, and in section 4, we will give our conclusions and recommendations for future laboratory studies.

2. Method

2.1. Experimental Setup

[9] *Vohl et al.* [1999] performed their experiment in the vertical wind tunnel of the Institute of Atmospheric Physics at the University of Mainz, Germany. *Pruppacher* [1988] and *Vohl* [1989] discuss technical details of the vertical wind tunnel. The experiment is described in detail in the study of Vohl et al. One large collector drop ($r > 50$ μm) was freely floating inside the vertical wind tunnel into which small droplets were injected. The collector drop grew by collision over a time period of 25 min either in laminar or in turbulent environment. To hold the growing collector drop stationary, the vertical velocity had to be increased accordingly. From the recorded air velocities, which are equivalent to the drop terminal velocities, the collector drop size could be calculated.

2.2. Model Calculations

[10] The growth rate of the suspended droplet with radius r_1 and mass m_1 is given by [*Vohl et al.*, 1999]:

$$\frac{\mathrm{d}r_1}{\mathrm{d}t} = \frac{r_1}{3m_1}\int_0^\infty K(r_1, r_2)g(r_2)\mathrm{d}r_2. \tag{1}$$

Here $K(r_1, r_2)$ is the coagulation kernel and $g(r_2)$ is the mass distribution function of the collected droplets. Depending on the state of the flow, K is either the sedimentation kernel for calm air, K_s, or is a modified kernel which accounts for the turbulence effects. Once $\mathrm{d}r_1/\mathrm{d}t$ is calculated, we integrate using a fourth-order Runge–Kutta scheme to obtain $r(t)$. In the following, we will discuss the assumptions and individual input parameters in more detail. The sedimentation kernel K_s for calm air is given by:

$$K_s(r_1, r_2) = \pi(r_1 + r_2)^2 E_s |v_T(r_1) - v_T(r_2)|. \tag{2}$$

Here E_s is the collection efficiency for calm air and $v_T(r_1)$ and $v_T(r_2)$ are the terminal velocities of the droplets in calm air.

[11] The collection efficiency E_s is determined by the collision efficiency $E_{col,s}$ and the coalescence efficiency $E_{coa,s}$ as $E_s = E_{col,s} \cdot E_{coa,s}$. For $E_{col,s}$, we use the values that are listed by *Vohl* [2000]. *Vohl et al.* [1999] further explore in their calculations, for the laminar cases, the differences between setting the coalescence efficiency $E_{coa,s} = 1$ and $E_{coa,s} < 1$. Since the differences between the two treatments are rather small and considering the uncertainty of the other input parameters, we set the coalescence efficiency both for the laminar case and the turbulent case to 1.

[12] Since a detailed description of the turbulent kernel is given by *Zhou et al.* [2001] and *Riemer and Wexler* [2005], we only summarize the main points. *Sundaram and Collins* [1997] show that the collision kernel in a turbulent fluid is of the form:

$$K_{t,0}(r_1, r_2) = \Gamma_0 \frac{\langle |w_r(r_1, r_2)| \rangle}{\langle |w_{r,\mathrm{shear}}(r_1, r_2)| \rangle} g_{12}(R), \tag{3}$$

where $R = r_1 + r_2$ is the collision radius and

$$\Gamma_0 = \sqrt{\frac{8\pi}{15}} R^3 \frac{v_k}{\eta}$$

is the collision kernel for zero-inertia particles according to the study of *Saffman and Turner* [1956], with the Kolmogorov velocity scale $v_k = (\nu\epsilon)^{\frac{1}{4}}$, where ν is the kinematic viscosity of the fluid ($\nu = 1.5 \cdot 10^{-5}$ m^2 s^{-1}). The Kolmogorov length scale is $\eta = (\nu^3/\epsilon)^{\frac{1}{4}}$. The angle brackets denote an ensemble average. $|w_r(r_1, r_2)|$ is the absolute value of the radial relative velocity between the two particles, and $|w_{r,\mathrm{shear}}(r_1, r_2)| = (2/15\pi)^{\frac{1}{2}} v_k (R/\eta)$.

[13] The factor $g_{12}(R)$ is the bidisperse radial distribution function at contact and accounts for the accumulation effect. *Zhou et al.* [2001] parameterize both terms based on the results of direct numerical simulations. The governing parameters are the Stokes numbers with respect to both the Kolmogorov timescale τ_k and the integral timescale T_e, and the Taylor-microscale Reynolds number $R_\lambda = u'\lambda/\nu$ where the transverse Taylor microscale is $\lambda = \sqrt{15\nu u'^2/\epsilon}$.

[14] With respect to the application to atmospheric conditions, the radial distribution function is a source of uncertainty since it is still an open question how the radial distribution function scales with R_λ. Direct numerical simulations can only be used to derive the scaling for the range of R_λ that can be covered with the simulations. Regarding this scaling, controversial results exist in the current literature. *Wang et al.* [2000] suggest a linear dependence of the radial distribution function on R_λ. On the other hand, *Collins and Keswani* [2005] find that the radial distribution function reaches a plateau with increasing R_λ. In any case, it remains uncertain how the scaling should be extrapolated to R_λ that are not accessible to direct numerical simulations.

[15] For the application of this concept to the experimental conditions, two issues need consideration. The solid line in Figure 1 shows an example of the data for the droplet growth under turbulent conditions as was measured

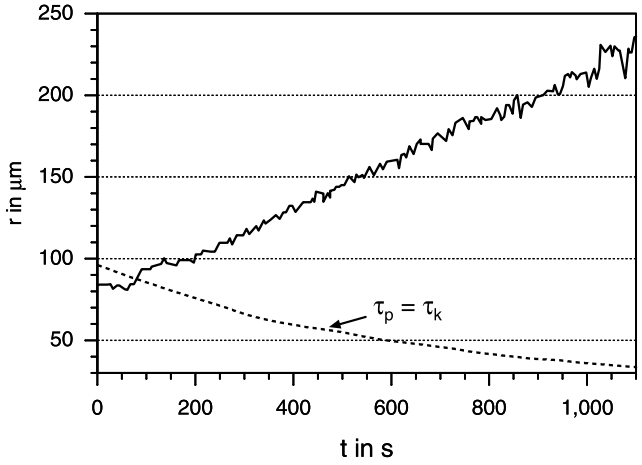

Figure 1. Comparison of the measured droplet growth (solid line) and calculated radius for which $St = 1$ (broken line).

by *Vohl et al.* [1999]. The broken line shows the droplet size $r_{crit} = \sqrt{9\rho\nu\tau_k/(2\rho_p)}$ for which the Stokes number with respect to the Kolmogorov timescale is one, with ρ being the air density and ρ_p the water density. Particles of this size are expected to be subject to preferential concentration.

[16] This size decreases since the dissipation rate is increasing over the course of the experiment, hence the curve diverges quickly from the curve that describes the growth of the collector drop. At the same time, the collected droplets with sizes smaller than 10 μm are smaller than both the collector drop and r_{crit}, hence for them preferential concentration does not apply either. In summary, this means that for the range of dissipation rates occurring in the experiment, the droplet sizes are never in a range where the accumulation effect plays a role, or, in other words, for the experimental conditions we find $g_{12} \approx 1$. Hence the aspect of the parameterization concerning the preferential concentration cannot be verified by the experimental data of Vohl et al., and this issue has to be deferred to future studies.

[17] Furthermore, the parameterization of *Zhou et al.* [2001] includes neither the hydrodynamic interactions nor the impact of gravity. In the atmosphere, clearly both turbulence and gravitation affect the size distribution, and hydrodynamic interactions occur. Therefore it is desirable to formulate a collision kernel that includes all of the above mechanisms. A quantitative framework starting from the first principle that deals with this issue is not yet available, therefore certain simplifying assumptions have to be made.

[18] The usual approach for modeling the impact of several coagulation mechanisms, such as for instance Brownian motion and gravitational settling, is to add the individual kernels. As *Butuirat and Kielkiewicz* [1996] show, this method gives satisfactory results. This superposition is justified in cases where the individual mechanisms act independently. If the accumulation effect was involved, the formulation of the resulting kernel would require more caution because sedimentation might counteract the clustering effect [*Vaillancourt and Yau*, 2000].

[19] However, since the droplets in the wind channel are quite large (> 50 μm), gravitational settling is in fact the dominant process. Turbulent coagulation supplies only a small contribution on top of this, by introducing additional relative velocities. This reason and the absence of the accumulation effect that we discussed above justify the approximation of using the sum of the sedimentation and turbulent kernels: $K_{tot} = K_s + K_t = E_s K_{s,0} + E_t K_{t,0}$. This means that we consider the two mechanisms independently and model the total kernel by superimposing the individual ones.

[20] The hydrodynamic interactions of droplets in turbulent flow are highly uncertain. There are indications that the collision efficiency is larger in turbulent air than in calm air [*Jonas and Goldsmith*, 1972; *Pinsky et al.*, 1999; *Wang et al.*, 2005], and it appears to be a random value ranging over a certain interval with a significant dispersion [*Pinsky et al.*, 1999]. Since a quantitative understanding of the dependency of the collision efficiency on turbulence intensity and different combinations of the colliding droplets is not yet established, for the purpose of this study, we will consider the two limiting cases of the collision kernel, i.e., (1) the case $E_t = 1$ and (2) the case $E_t = E_s$.

[21] *Vohl et al.* [1999] state that the laminar collision kernel had to be increased by 10–20% to obtain a good agreement between calculation and experiment under turbulent conditions. We realize that with the information from this experiment, it is not possible to attribute this overall increase to an increase in the collision efficiency and/or an increase in the geometric collision kernel; however, in the absence of other data sources, we still find it worthwhile to compare the data with the theory as they are available to date, and we will address the uncertainties with sensitivity calculations.

[22] To employ the formulation of the collision kernel according to the study of *Zhou et al.* [2001], we need to know the size distribution of the collected drops, the dissipation rate, and the r.m.s. velocity fluctuations of the tunnel flow. From the experiment, we extract the following information (data reproduced from the original paper by *Vohl et al.* [1999]):

2.2.1. Droplet Size Distribution

[23] In their paper, *Vohl et al.* [1999] give examples of typical droplet spectra sampled over 10-s intervals and for the liquid water content. The shape of the individual droplet spectra varies slightly but remains roughly the same over the whole sampling period. Figure 2 gives the mean mass size distribution and the variability (maximum and minimum values). Figure 3 shows that the liquid water content decreases over time. To generate the droplet spectrum of the collected droplets at each time step, we therefore multiply the normalized droplet spectra by the liquid water content that corresponds to the individual time. To account for the variations of the droplet spectra shape we cycle through six spectra every 60 s, 10 s per spectrum, to inject a small amount of noise into the simulation. Compared to using the average, this did not have a large effect. Results presented here are with the cycling.

2.2.2. Dissipation Rate ϵ

[24] As the suspended droplet grows and the mean velocity increases, the dissipation rate also increases over the course of the experiment. At three mean velocities (0.5 m s^{-1}, 1.05 m s^{-1}, and 1.77 m s^{-1}), dissipation rates were measured to be 10 cm^2 s^{-3}, 100 cm^2 s^{-3}, and

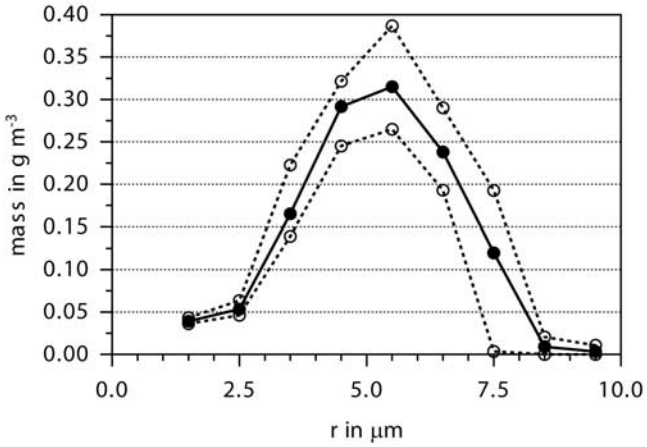

Figure 2. Mass distributions of the collected droplets. Solid line represents the mean spectrum while broken lines show the variability.

700 cm^2 s^{-3} [*Vohl*, 2000]. Since the mean velocities are equivalent to the drop terminal velocity, we can infer the corresponding radius of the suspended droplet. To obtain dissipation rate values in-between the three data points, we fit the data with the function $\epsilon = Ar^b$ with $A = 1.04 \cdot 10^{-11}$ and $b = 4.2$ as shown in Figure 4.

2.2.3. R.m.s. Velocity u'

[25] *Vohl* [2000] gives values for the degree of isotropic turbulence T^* for different mean velocities. Since T^* is defined as $T^* = \sqrt{u'^2}/\bar{u}$, u' can be directly derived. The values are displayed in Figure 4 along with the linear regression, which we use to obtain u' for any radius.

3. Results

[26] In this section, we compare the simulations to the measurements addressing uncertainties in the input data with sensitivity calculations. *Vohl et al.* [1999] have performed two turbulent growth experiments that lasted for a full period of about 20 min. They refer to them as experiments 'Drop 2' and 'Drop 7', and we will adopt those terms here.

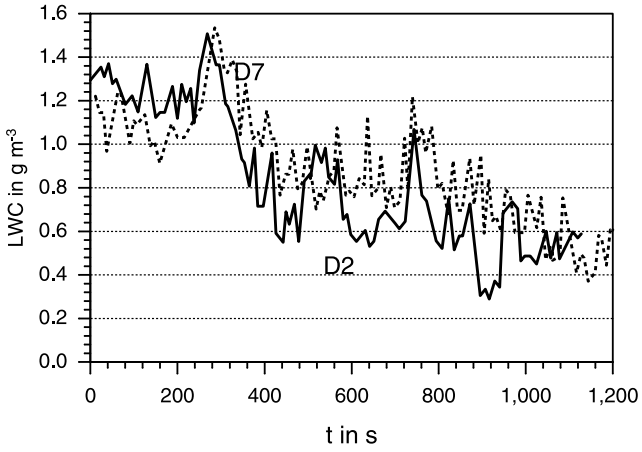

Figure 3. Liquid water content of the growth experiments 'Drop 2' (solid line) and 'Drop 7' (dotted line).

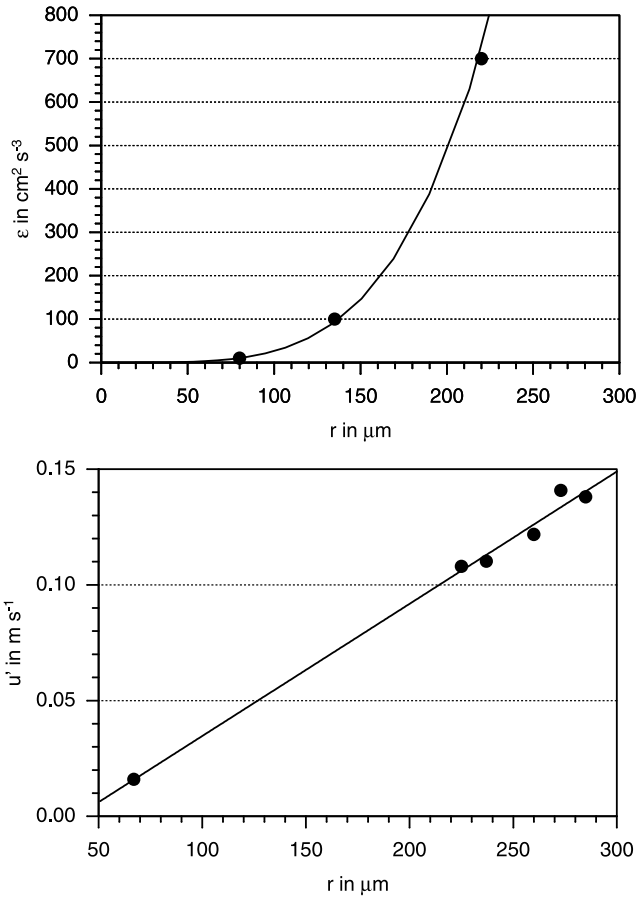

Figure 4. Measured dissipation rates (top) and r.m.s. velocity fluctuations (bottom) for varying drop radii.

[27] The solid line in Figure 5 shows the growth of the collector droplet for the experimental data of run 'Drop 2' [*Vohl et al.*, 1999] and the dotted line represents the calculation assuming laminar flow. For this calculation, we used the collision kernel K_s according to equation (2). The corresponding figure for the experiment 'Drop 7' is shown in Figure 6. As already concluded by *Vohl et al.* [1999], the laminar calculation cannot reproduce the turbulent measurements. The other lines represent the calculations with the kernel including turbulence (K_{tot}) as outlined above and explore the sensitivity to the size distribution of the collected droplets and the assumption about E_t. The inset shows the second half of the experiment in more detail.

[28] In Figure 5, Curve 1 shows the predictions with the size distribution of the collected droplets according to Figure 2 and the parameters ϵ and u' varying as shown in Figure 4, which represents our best estimate of these quantities. Additionally, we assume $E_t = E_s$. The result confirms our expectation that using the assumption $E_t = E_s$ results in a lower limit for the droplet growth, underestimating the data. On the other hand, if we assume $E_t = 1$, we obtain Curve 2, which lies in the range of the measurements. We repeated these calculations with an increased number of collected droplets in the last two bins and show the results as Curve 3 ($E_t = E_s$) and Curve 4 ($E_t = 1$). The average mass density was increased from $9.1 \cdot 10^{-3}$ g m^{-3}

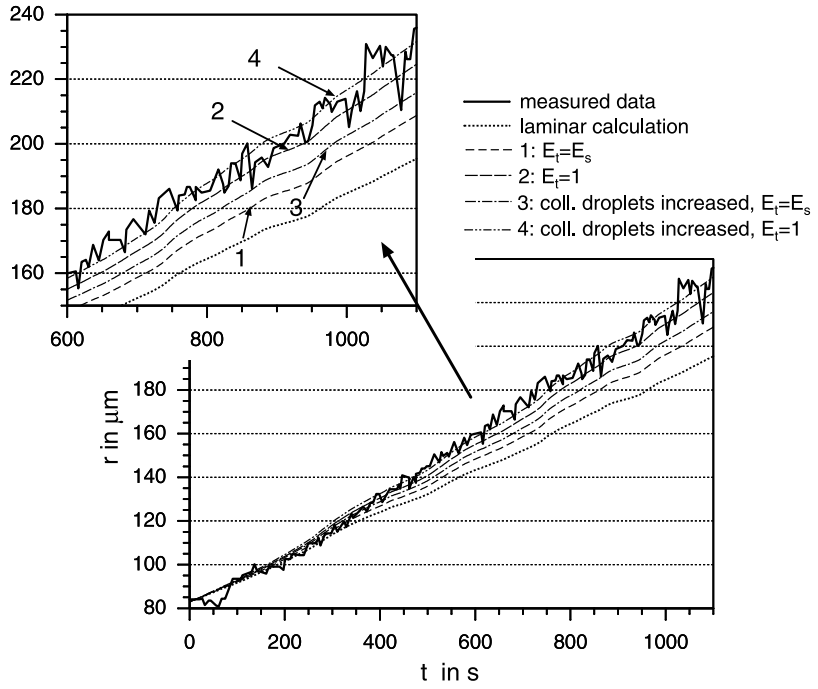

Figure 5. Comparison of the experimental turbulent drop growth data ('Drop 2') with model results.

to $1.7 \cdot 10^{-2}$ g m^{-3} (second last bin) and from $3.4 \cdot 10^{-3}$ g m^{-3} to $2.3 \cdot 10^{-2}$ g m^{-3} (last bin). For these calculations, the growth is increased since more larger droplets are available for collection, but the results are not qualitatively different from Curves 1 and 2.

[29] We conclude from these calculations that, at least for the given conditions, the sensitivity toward the exact value of E_t is rather limited compared to the sensitivity to changes in the droplet size distribution. A slight change in the droplet size distribution (relative contribution of the number of largest droplets increased by about 10%, which corresponds to the range of uncertainty of the measurements) is as important as varying the collision efficiency between the two extreme values. As long as $E_t > E_s$, we obtain results in the range of the experimental data. Since E_t is such a highly uncertain parameter, we will assume

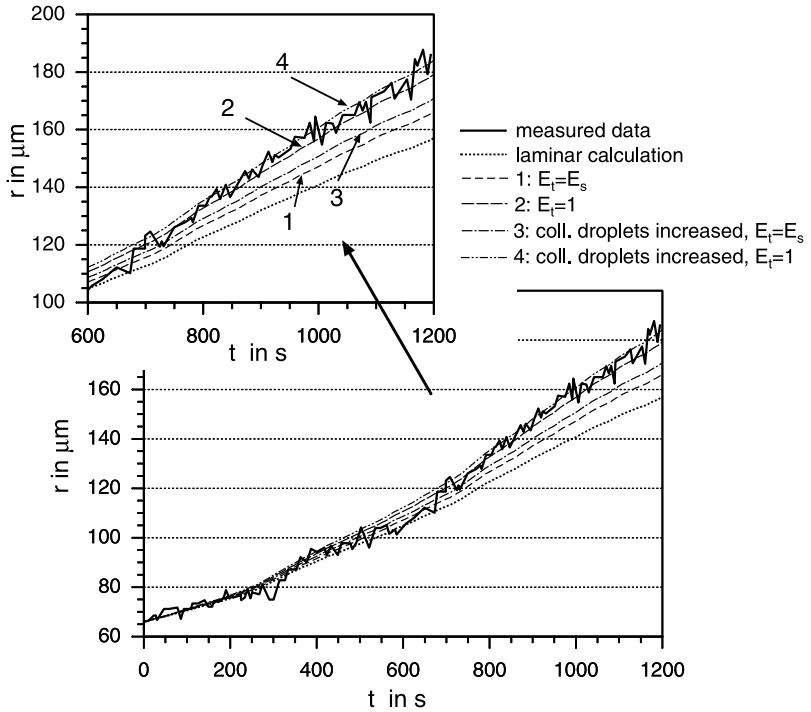

Figure 6. Same as Figure 5 but for the experiment 'Drop 7'.

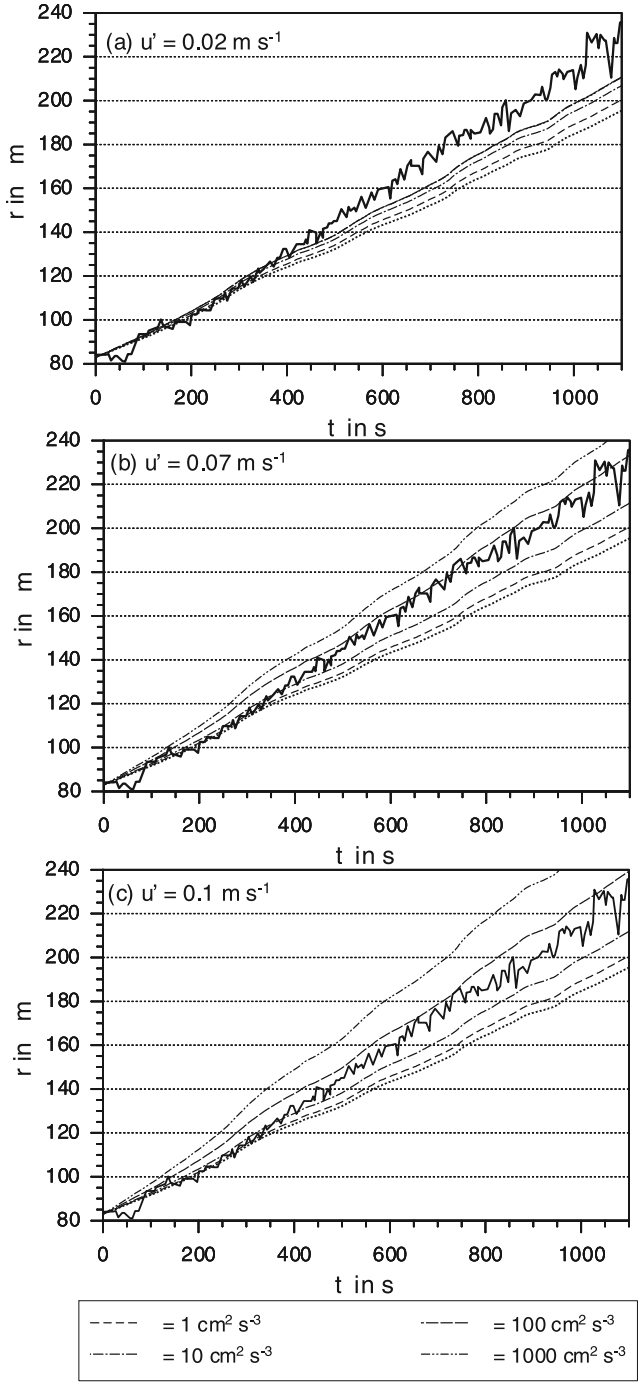

Figure 7. Sensitivity calculations with constant values for u' and ϵ. Solid line: data ('Drop 2'), dotted line: calculation assuming laminar flow. The other lines represent a specific value for ϵ. From bottom to top: $\epsilon = 1$ cm^2 s^{-3}, 10 cm^2 s^{-3}, 100 cm^2 s^{-3}, 1000 cm^2 s^{-3}. (a) $u' = 0.02$ m s^{-1}, (b) $u' = 0.07$ m s^{-1}, (c) $u' = 0.1$ m s^{-1}.

$E_t = 1$ for the following discussion and keep in mind that the results represent an upper estimate. The same argument applies to the second droplet growth experiment ('Drop 7') shown in Figure 6.

[30] While in Figures 5 and 6 the parameters ϵ and u' were allowed to vary as it was the case in the experiment, we also want to show results for different but constant turbulent conditions to shed light on the influence of ϵ and u'.

[31] Figures 7a–7c show again the results for the 'Drop 2' data (solid line: data, dotted line: laminar calculation for reference). The values for u' and ϵ were held constant at $u' = 0.02$ m s^{-1}, $u' = 0.07$ m s^{-1}, and $u' = 0.1$ m s^{-1}, respectively. The individual curves represent the dissipation rates $\epsilon = 1$ cm^2 s^{-3}, 10 cm^2 s^{-3}, 100 cm^2 s^{-3}, and 1000 cm^2 s^{-3}. For $u' = 0.02$ m s^{-1}, the agreement of calculations and measurements are good at the start; however, for times $t > 500$ s, the calculations deviate more and more from the experimental results since the calculated growth rate is too small for all values of ϵ. For $u' = 0.07$ m s^{-1} and $u' = 0.1$ m s^{-1}, the calculated growth rate is too small during the second half of the experiment for $\epsilon = 1$ cm^2 s^{-3} and $\epsilon = 10$ cm^2 s^{-3}, or it is too large for the entire time, resulting in an overestimation of the droplet growth ($\epsilon = 100$ cm^2 s^{-3} and $\epsilon = 1000$ cm^2 s^{-3}). The comparison of the figures also shows that the sensitivity to ϵ is dependent on u'. The smaller u', the smaller is the response to changes in ϵ. For $u' = 0.02$ m s^{-1}, a limit of the sensitivity to ϵ has been reached. Please note that the curves for $\epsilon = 100$ cm^2 s^{-3} and $\epsilon = 1000$ cm^2 s^{-3} are visually indistinguishable. We can explain this by the fact that $\langle |w_r(r_1, r_2)| \rangle / \langle |w_{r,\mathrm{shear}}(r_1, r_2)| \rangle \rightarrow 1$ for $\epsilon \rightarrow \infty$. The turbulent kernel K_t then varies proportionally to Γ_0, which is only weakly dependent on ϵ. This limiting behavior has not been reached yet for the cases $u' = 0.07$ m s^{-1} and $u' = 0.1$ m s^{-1}.

[32] In summary, these sensitivity calculations show that the variation of the parameters ϵ and u' leads to a pronounced response in the calculated results. For a fixed u', the sensitivity to ϵ depends on the magnitude of u' (the larger u', the larger the sensitivity to ϵ). The duration of the experiments of about 20 min is obviously a valuable feature since the divergence of the individual runs from each other and the observations frequently only appear after about 400 s. We also conclude that arbitrarily chosen values do not reproduce the experimental values to the same extent as our best estimate does (cf. Figures 5 and 6).

[33] For atmospheric conditions, the energy dissipation rates are comparable to those of the experiment but the associated r.m.s. velocities are expected to be higher in the atmosphere, roughly following the scaling relationship $\epsilon \sim u'^3/L$ with L being the typical length scale [*MacPherson and Isaac*, 1977]. If we assume $L = 1000$ m and $\epsilon = 100$ cm^2 s^{-3}, we obtain $u' = 2.15$ m s^{-1}, a value which is in the range of the in-cloud measurements by *MacPherson and Isaac* [1977]. Figure 8 illustrates the effect if we increase the r.m.s. velocity to atmospheric values. The solid line is again the experimental data 'Drop 2', the filled circles represent the calculation when $\epsilon = 100$ cm^2 s^{-3} and r.m.s. velocity fluctuation to $u' = 2$ m s^{-1} which is one magnitude larger than in the experiment and more realistic for real, atmospheric conditions.

[34] Growth is enhanced compared to the laboratory experiment suggesting that in the atmosphere the turbulence enhancement is likely to be larger than observed in the experiment, even without preferential concentration being an important factor. An additional phenomenon, which cannot be addressed with wind tunnel studies, is the intermittent turbulence structure in clouds, characteristic for high Reynolds number atmospheric flow. As in-cloud measurements by *Siebert et al.* [2006] show, maximum

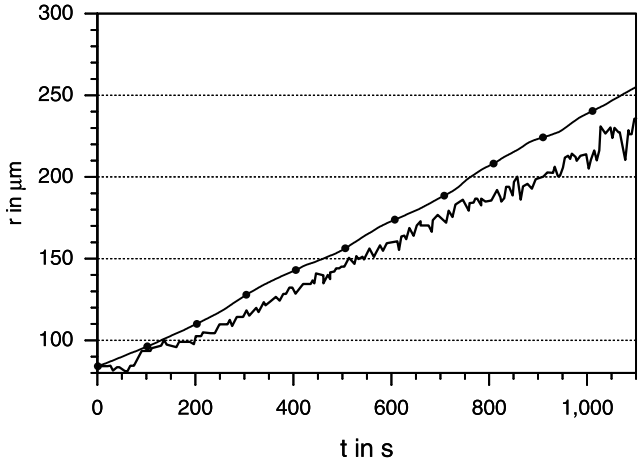

Figure 8. Solid line: data, circles: expected growth for atmospheric conditions with $\epsilon = 100\ \mathrm{cm^3\ s^{-2}}$ and $u' = 2\ \mathrm{m\ s^{-1}}$.

values of ϵ can be on the order of two magnitudes higher than the mean value. This means that for atmospheric conditions where intermittency occurs, the use of mean values for ϵ may lead to an underestimation of the turbulence effect.

4. Conclusions

[35] We compare the drop growth measurements from the study of *Vohl et al.* [1999] with numerical results based on the model for the turbulent kernel by *Zhou et al.* [2001]. As shown in this experiment, the drop growth under turbulent conditions proceeds faster than under laminar conditions and it hence cannot be reproduced by calculations that only use the well-established sedimentation kernel.

[36] We present an approach for combining the turbulent kernel and the sedimentation kernel to obtain an overall one, which depends on u' and ϵ. Sensitivity calculations show that u' and ϵ are in fact important parameters, which influence the results considerably. We want to emphasize that the experiments represent a special case, i.e., a large collector drop that is exposed to a cloud of small collected droplets. For these conditions, turbulence only provides a small enhancement to the gravitational kernel. Our results show that the overall kernel describes the growth adequately. Since the design of the experiment does not allow the verification of the radial distribution function parameterization of *Zhou et al.* [2001], we recognize that this study is only one step toward validating the complete kernel. Further validation awaits suitable data.

[37] From our sensitivity calculations, we conclude that in order to validate model calculations with laboratory experiments, it is important to:

[38] (1) Characterize the droplet spectrum accurately, especially with respect to the larger sizes since they are the key drivers of droplet growth.

[39] (2) Characterize the turbulence parameters u' and ϵ accurately. The higher u', the more sensitive is the result to ϵ.

[40] (3) Perform measurements for long-enough time periods so that laminar and turbulent conditions lead to clearly different results.

[41] (4) Explore different Stokes number regimes to include the potential impact of clustering on droplet growth.

References

Arenberg, D. (1939), Turbulence as the major factor in the growth of cloud drops, *Bull. Am. Meteorol. Soc.*, *20*, 444–448.

Butuirat, F., and M. Kielkiewicz (1996), On additivity of coagulation kernels, *Ann. Nucl. Energy*, *23*, 1091–1096.

Collins, L., and A. Keswani (2005), Reynolds number scaling of particle clustering in turbulent aerosols, *New J. Phys.*, *6*, 119.

Frehlich, R., Y. Meillier, M. L. Jensen, and B. Balsley (2004), A statistical description of small-scale turbulence in the low-level nocturnal jet, *J. Atmos. Sci.*, *61*, 1079–1085.

Jonas, P., and P. Goldsmith (1972), The collection efficiencies of small droplets falling through a sheared air flow, *J. Fluid Mech.*, *52*, 593–608.

Kruis, F., and K. Kusters (1996), The collision rate of particles in turbulent media, *J. Aerosol Sci.*, *27*, S263–S264.

MacPherson, J., and G. Isaac (1977), Turbulent characteristics of some Canadian cumulus clouds, *J. Appl. Meteorol.*, *16*, 81–90.

Maxey, M. (1987), The gravitational settling of particles in homogeneous turbulence and random flow fields, *J. Fluid Mech.*, *174*, 441–465.

McGraw, R., and Y. Liu (2004), Analytic formulation and parameterization of the kinetic potential theory for drizzle formation, *Phys. Rev. E*, *70*, 031606.

Pinsky, M., A. Khain, and M. Shapiro (1999), Collision of small drops in a turbulent flow. part I: Collision efficiency. Problem formulation and preliminary results, *J. Atmos. Sci.*, *56*, 2585–2600.

Pruppacher, H. (1988), Auswaschen von atmosphärischen Spurenstoffen durch Wolken und Niederschlag mittels eines vertikalen Windkanals, *Tech. rep.*, BPT-Bericht 9/88, available from G.S.F. Forschungszentrum Neuherberg, Ingoldstädter Landstr. 1, 85764 Oberschleissheim, Germany.

Riemer, N., and A. Wexler (2005), Droplets to drops by turbulent coagulation, *J. Atmos. Sci.*, *62*, 1962–1975.

Saffman, P., and J. Turner (1956), On the collision of drops in turbulent clouds, *J. Fluid Mech.*, *1*, 16–30.

Shaw, R. (2003), Particle-turbulence interactions in atmospheric clouds, *Annu. Rev. Fluid Mech.*, *35*, 183–227.

Siebert, H., K. Lehmann, and M. Wendisch (2006), Observations of small scale turbulence and energy dissipation rates in the cloudy boundary layer, *J. Atmos. Sci.*, *63*, 1451–1466.

Sundaram, S., and L. Collins (1997), Collision statistics in an isotropic, particle-laden turbulent suspension. part I: Direct numerical simulations, *J. Fluid Mech.*, *335*, 75–110.

Vaillancourt, P., and M. Yau (2000), Review of particle-turbulence interactions and consequences for cloud physics, *Bull. Am. Meteorol. Soc.*, *81*, 285–298.

Vohl, O. (1989), Die dynamischen Charakteristika des Mainzer vertikalen Windkanals, Master's thesis, Institute of Atmospheric Physics, Johannes Gutenberg University, Mainz, Germany.

Vohl, O. (2000), *An Experimental Investigation of the Effects of Turbulence on the Scavenging of Aerosol Particles by Rain Drops, and on the Growth of Cloud Drops by Collision*, Shaker-Verlag, Aachen, Germany, ISBN 3-8265-8210-1.

Vohl, O., S. Mitra, S. Wurzler, and H. Pruppacher (1999), A wind tunnel study of the effects of turbulence on the growth of cloud drops by collision and coalescence, *J. Atmos. Sci.*, *56*, 4088–4099.

Wang, L.-P., A. Wexler, and Y. Zhou (2000), Statistical mechanical description and modelling of turbulent collision of inertial particles, *J. Fluid Mech.*, *415*, 117–153.

Wang, L.-P., O. Ayala, S. Kasprzak, and W. Grabowski (2005), Theoretical formulation of collision rate and collision efficiency of hydrodynamically-interacting cloud droplets in turbulent atmosphere, *J. Atmos. Sci.*, *62*, 2450–3243.

Zhou, Y., A. Wexler, and L.-P. Wang (2001), Modelling turbulent collision of bidisperse inertial particles, *J. Fluid Mech.*, *433*, 77–104.

K. Diehl, Institute of Atmospheric Physics, Johannes Gutenberg University, Mainz, Germany.

N. Riemer, Marine Sciences Research Center, Stony Brook University, Stony Brook, NY 11794-5000, USA. (nicole.riemer@stonybrook.edu)

A. S. Wexler, Department of Mechanical and Aeronautical Engineering, University of California, Davis, CA 95616, USA.